Algorithms for the inversion of lidar signals: Rayleigh-Mie measurements in the stratosphere

Fabrizio Masci
Istituto Nazionale di Geofisica, L'Aquila, Italy

Abstract
We report the features and the performances of the algorithms, developed at the Lidar Station of L'Aquila, for retrieving atmospheric parameters and constituents from elastic lidar signals. The algorithm for ozone retrieving is discussed in detail and checked with model lidar signals to take into account the numerical distortion on the profile. The performances of the aerosol backscattering ratio algorithm that includes the transmission loss due to the aerosol extinction are evaluated. A new algorithm developed to retrieve atmospheric temperature profiles from elastic lidar returns in the altitude range 30-90 km is also examined in detail.

Key words *lidar – dial – ozone – aerosol – temperature*

1. Introduction

The Lidar Station of L'Aquila (SLAQ) (located 42.35°N, 13.33°E, and 683 m above sea level) includes two lidar systems: a DIAL (DIfferential Absorption Lidar) ozone system and a Rayleigh-Mie lidar. The source of the dial system is an excimer laser emitting pulses at 308 nm and 351 nm wavelengths. Until March 1993, the Rayleigh-Mie lidar used a dye laser emitting pulses at 589 nm wavelength. At the end of 1993 this laser was replaced with a Nd-Yag laser which emits pulses at 532 nm wavelength (2nd harmonic). For system details refer to D'Altorio *et al.* (1992) and Di Carlo *et al.* (1998). The two systems have been operating simultaneously since summer 1991 monitoring the ozone concentration in the stratosphere (Masci *et al.*, 1991) and the Pinatubo aerosol cloud (D'Altorio *et al.*, 1993a,b). Both the lidars were also involved in comparison campaigns with instruments mounted on satellites (Redaelli *et al.*, 1994; Yue *et al.*, 1995) and Space Shuttle (Rizi *et al.*, 1996). The significance of ozone concentration profiles, aerosol backscattering ratio profiles and temperature profiles in the lower and upper stratosphere are assessed for test cases. The errors on the measurements and the distortions on the retrieved profiles due to the algorithms are also discussed.

Mailing address: Dr. Fabrizio Masci, Istituto Nazionale di Geofisica, Castello, 67100 L'Aquila, c/o Dipartimento di Fisica, Facoltà di Scienze, Università di L'Aquila, Via Vetoio 10, 67010 Coppito, L'Aquila; e-mail: masci@aquila.infn.it

2. DIAL ozone algorithm

The differential absorption lidar technique is a powerful method for measuring stratospheric ozone profiles with high temporal and spatial resolution. The elastic scattering lidar equation, in single scattering approximation, can be written as follows

$$S_\lambda(z) = \frac{k_\lambda}{z^2}\beta_\lambda(z)\exp[-2\tau_\lambda(z)] \qquad (2.1)$$

where $S_\lambda(z)$ is the lidar return signal at wavelength λ from range z, k_λ is the lidar system constant, $\beta_\lambda(z)$ is the total atmospheric volume backscatter coefficient, and $\tau_\lambda(z)$ is the total atmospheric optical depth. The total atmospheric optical depth $\tau_\lambda(z)$ can be written as follows

$$\tau_\lambda(z) = \int_0^z [\alpha_\lambda(z') + n_{oz}(z')\,\sigma_\lambda(T)]\,dz' \quad (2.2)$$

where $a_\lambda(z)$ is the total atmospheric extinction coefficient excluding ozone absorption, $n_{oz}(z)$ is the ozone number density, and $\sigma_\lambda(T)$ is the ozone absorption cross section at temperature T. The T dependence with z is implicit. The total atmospheric volume backscatter coefficient $\beta_\lambda(z)$ can be written as follows

$$\beta_\lambda(z) = \beta_{a,\lambda}(z) + \frac{3}{8\pi}\sigma_{R,\lambda}\rho(z) \quad (2.3)$$

where $\beta_{a,\lambda}(z)$ is the aerosol volume backscatter coefficient, $\sigma_{R,\lambda}$ is the Rayleigh scattering cross section at wavelength λ, and $\rho(z)$ is the molecular number density. Rayleigh cross sections and ozone absorption cross sections are available from literature (Bucholtz, 1995; Malicet *et al.*, 1995), while the atmospheric density profiles are available from local radiosonde soundings or atmospheric models (*i.e.* US Standard Atmosphere, CIRA). Here are shown only the effects on retrieved ozone profile of the dial signals inversion procedure referring to other papers for the interference due to the aerosol presence (D'Altorio *et al.*, 1992, 1993a,b; Steinbrecht and Carswell, 1995). When the aerosol contribution is negligible, no contribution of aerosol either in term of backscattering or extinction can be assumed, so the eq. (2.2) reduces to

$$\tau_\lambda(z) = \int_0^z [\rho(z')\sigma_{R,\lambda} + n_{oz}(z')\sigma_\lambda(T)]dz' \quad (2.4)$$

and the eq. (2.3) reduces to

$$\beta_\lambda(z) = \frac{3}{8\pi}\sigma_{R,\lambda}\rho(z). \quad (2.5)$$

Then $S'_\lambda(z)$ can be defined as the signal corrected from the molecular extinction, obtained by $S_\lambda(z)$ knowing the atmospheric density profile, as follows

$$S'_\lambda(z) = z^2\, S_\lambda(z) \exp\left[2\sigma_{R,\lambda}\int_0^z \rho(z')\,dz'\right]. \quad (2.6)$$

Combining the previous expression with the eqs. (2.1), (2.4) and (2.5), $S'_\lambda(z)$ can be rewritten

$$S'_\lambda(z) = k_\lambda \frac{3}{8\pi}\sigma_{R,\lambda}\rho(z)\cdot \cdot\exp\left[-2\int_0^z n_{oz}(z')\sigma_\lambda(T)\,dz'\right]. \quad (2.7)$$

With the dial technique an ozone profile can be obtained taking measurements at two wavelengths in the ozone UV absorption band: one with a strong ozone absorption, the so called *on* wavelength (308 nm for SLAQ), and the other with a lower ozone absorption, the so called *off* wavelength (351 nm for SLAQ), which is used a reference signal. The ozone profile can be obtained making the derivative respect z of the logarithm of ratio between the *on* and the *off* signals. Then the ozone density profile is given by

$$n_{oz}(z) = -\frac{1}{2\Delta\sigma(T)}\frac{d}{dz}Y(z) \quad (2.8)$$

where

$$\Delta\sigma(T) = \sigma_{on}(T) - \sigma_{off}(T)$$

and

$$Y(z) = \ln\left[\frac{S'_{on}(z)}{S'_{off}(z)}\right]. \quad (2.9)$$

Since the lidar signals from the higher altitude are weaker, their signal-to-noise ratios are smaller, and the statistical errors increase with altitude. The statistical error can be reduced using

a smoothing procedure on the function $Y(z)$. This consists in a running polynomial fitting of the function $Y(z)$. At the range z the fitting of $Y(z)$ is applied over a number $N(z)$ of cells above and below z. The number $N(z)$ increases with z to take into account the decreasing of the signal-to-noise ratio. The data are fitted in a weighted least-squares sense. The weights of the fit are the variances of $Y(z)$ obtained by propagating the variance of all the terms appearing in the eq. (2.9). If m is the fitting polynomial order, $Y(z)$ can be written as

$$Y(z) = \sum_{j=0}^{m} a_j z^j \qquad (2.10)$$

where a_j are the polynomial coefficients.

In this case the derivative can be applied to the fitting function, so the eq. (2.8) can be re-written as follows

$$n_{oz}(z) = -\frac{1}{2\Delta\sigma(T)} \sum_{j=1}^{m} j a_j z^{j-1}. \qquad (2.11)$$

The ozone standard deviation is given by

$$\sigma^2_{n_{oz}}(z) = \left[\frac{1}{2\Delta\sigma(T)}\right]^2 \left\{\sum_{j=1}^{m} (jz^{j-1})^2 \sigma^2_{\alpha_j} + \right. \qquad (2.12)$$

$$\left. + 2\sigma^2_{a_1,a_2} \left[\frac{\partial n_{oz}(z)}{\partial a_1}\right]\left[\frac{\partial n_{oz}(z)}{\partial a_2}\right] + \ldots\ldots \right\}$$

where $\sigma^2_{a_j}(z)$ and $\sigma^2_{a_j,a_i}(z)$ are the variances and the covariance of the polynomial coefficients respectively. The number of the terms in eq. (2.12) involving the covariance of the polynomial coefficients depends on the fitting polynomial order. In any case the smoothing procedure decreases the statistical error, but causes a distortion on the ozone profile. This distortion is one of the systematic errors which is characteristic of the dial ozone algorithm. To illustrate this point more clearly dial signals have been simulated using the US Standard Atmosphere temperature and pressure profiles and a synthetic ozone profile. In this simulation no aerosol term has been considered and random noise was added to simulate the statistical fluctuation of the signals. The left panel of fig. 1 shows the synthetic ozone profile used for the simulation and the retrieved ozone profiles for three different order of the polynomial fitting procedures. The right panel shows the percentage differences of the retrieved ozone profiles with respect to the synthetic profile. This simulation shows that the 3rd order polynomial fitting distorts the retrieved ozone profile less than the lower order polynomial fitting procedures except for the higher altitude where the signal-to-noise ratios of the dial signals are lower. From fig. 1 it can be noted that the 3rd order polynomial fitting shows good results when a thin layer is present in the ozone profile as can be seen at the altitude range 11-13 km. The 1st and the 2nd order polynomial fittings show similar results in the lower altitudes, whereas the 2nd order polynomial fitting has a better behaviour with respect to the 1st order for higher altitudes. So taking into account only the algorithm's distortion on the retrieved ozone profile, the 3rd order polynomial fitting seems to have a better behaviour except when the signal-to-noise ratio becomes low. Figure 2 shows the dial ozone profile obtained on May 10, 1994. In SLAQ each ozone profile is obtained with two sessions of measurements: a Low Session (LS) in the 10-30 km altitude range, and a High Session (HS) in the 25-45 km altitude range. The final ozone profile is obtained merging the LS profile and the HS profile in the overlap altitude range (typically around 25-30 km). The left panel of the figure shows the ozone profiles obtained by the three different fitting procedures compared with an ozonesonde sounding (ECC) effectuated at SLAQ in the same time period of the lidar measurement. The right panel of the figure shows the errors (1σ standard deviation) of the ozone values for the three different fitting procedures. Even if the 3rd order polynomial fitting shows good results in the altitude range (12-14 km) where a thin ozone layer is present, it distorts the ozone profile when the signal to noise-ratio becomes low, as can be seen in the upper part of the LS profile (17-25 km). In any case the error on the retrieved ozone profile, when a 3rd order polynomial fitting is applied, is up to four times

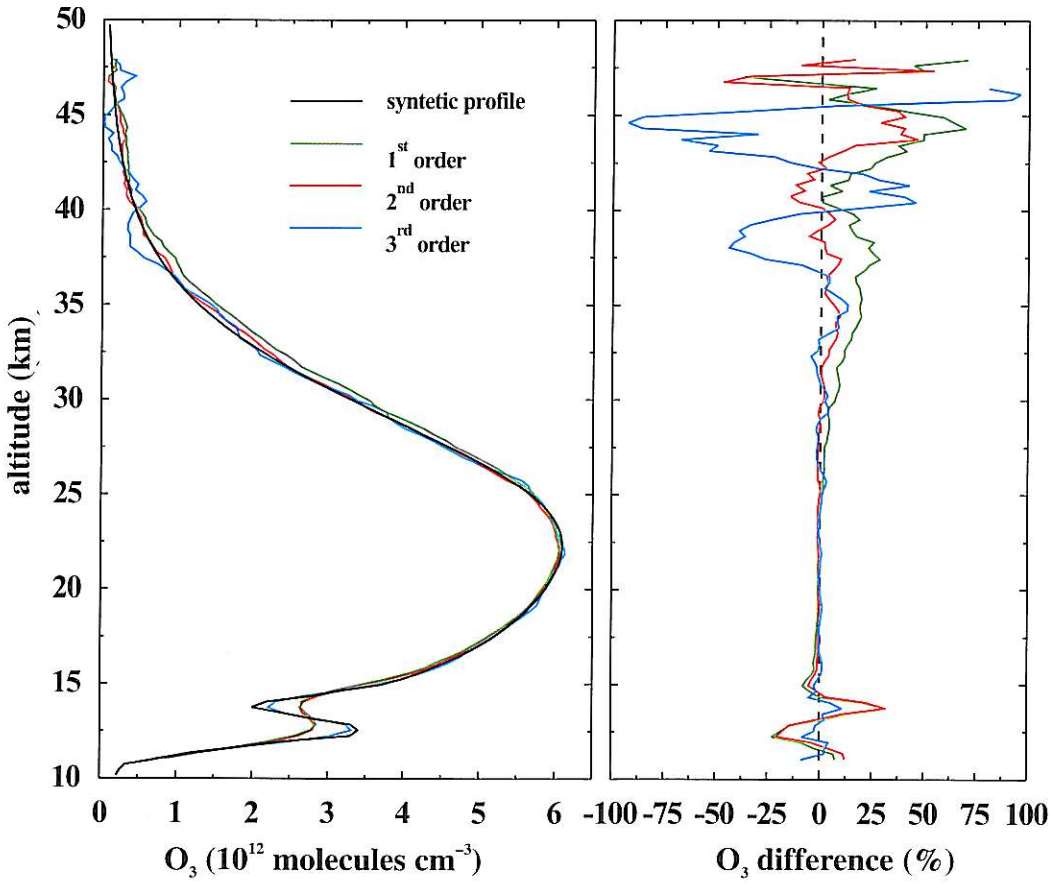

Fig. 1. *Left:* dial ozone profiles, obtained by the model dial signals using three different fitting procedures, compared with the synthetic ozone profile. *Right:* percentage differences between the three retrieved ozone profiles and the synthetic ozone profile.

higher than the lower order polynomial fitting procedures. Therefore the 3rd order polynomial fitting distorts the ozone profile less when the signal-to-noise ratio is high, as can been seen in the previous simulation, but introduces a high error on the retrieved ozone values. So, a good compromise between low distortion of the ozone profile and low error on ozone values is obtained by fitting the function $Y(z)$ with a 2nd order polynomial.

Applying on the function $Y(z)$ a smoothing procedure and the derivative corresponds to weight $Y(z)$ with a low-pass derivative numerical filter. The coefficients of this filter for a 2nd order polynomial fitting procedure are given by Godin (1987). The cut-off frequencies $v_c(z)$ of the numerical filter determine the range resolution $Z_R(z)$ of the ozone profile according to

$$Z_R(z) = \frac{\Delta z}{v_c(z)} \qquad (2.13)$$

where Δz is the range cell width. For SLAQ lidar systems Δz = 0.3 km. The right panel of fig. 2 shows also the range resolution of the

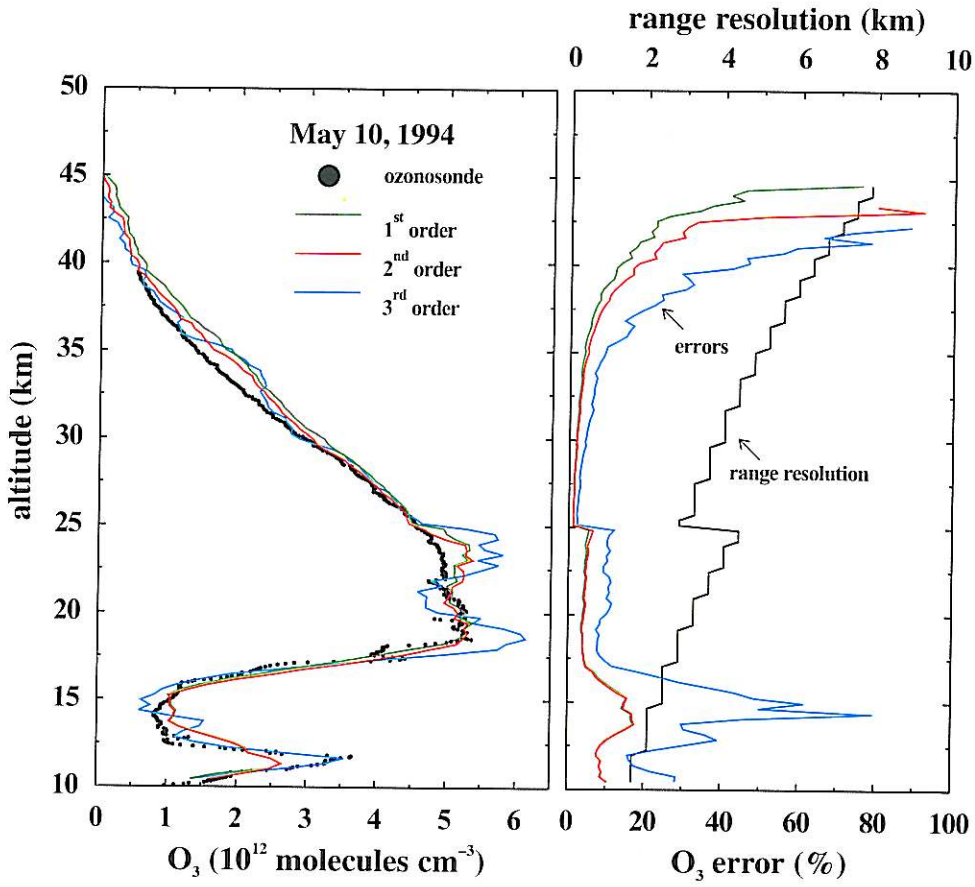

Fig. 2. *Left:* May 10, 1994 dial ozone profiles retrieved using the three different smoothing procedures compared with the ozonesonde profile of the same day. *Right:* error (1σ standard deviation) and range resolution of the ozone profile.

ozone profile. In fig. 2 the dial ozone profile is compared with an ozonesonde sounding. In this comparison there are two kinds of problems. First of all the ozonesonde samples different air masses respect to the lidar. Then the range resolution of the ozonesonde sounding is about ten times higher than the lidar measurement. To compare the two measurements the range resolution of the ozonesonde profile can be reduced to the range resolution of the dial ozone profile. A first step is to reduce the range resolution of the ozonesonde profile to the dial signals resolution Δz. After that, to have on the ozonesonde profile a similar smoothing of the dial ozone profile, a low-pass filter (*i.e.* 2nd order polynomial filter) with the same cut-off frequencies $\nu_c(z)$ should be applied on the ozonesonde profile. Figure 3 reports the transmission function of the low-pass filter equivalent to the 2nd order polynomial derivative filter for $N = 3$. It also reported the low-pass 2nd order polynomial filter for $N = 5$ which has the same cut-off frequency as the previous filter. From fig. 3 it can be noted that the two filters are similar but not equal. Near the cut-off frequency ν_c the transmission functions have a different slope so the two fil-

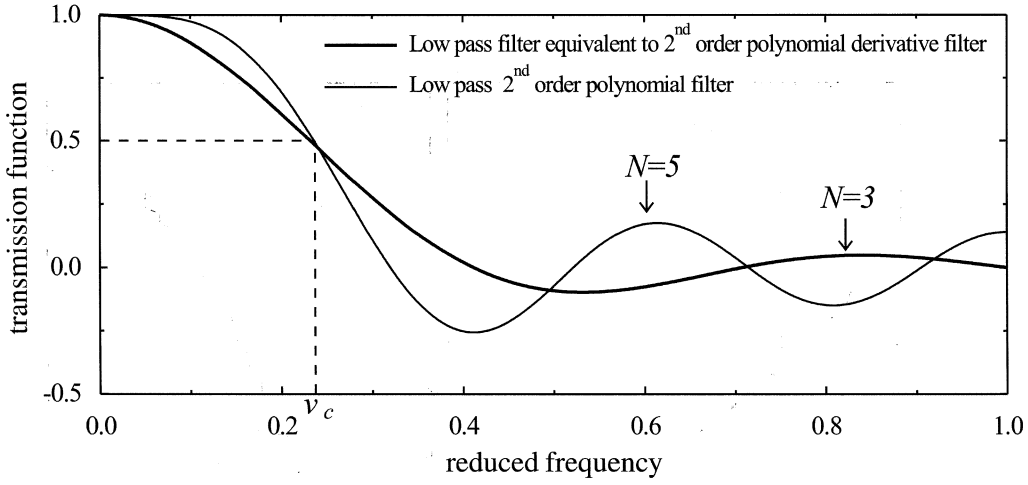

Fig. 3. Transmission functions of the low-pass filter equivalent to the 2nd order polynomial derivative filter for $N = 3$ and the 2nd order polynomial low-pass filter for $N = 5$. The common cut-off frequency v_c is 0.23.

ters have a different behaviour at the intermediate frequencies. While, for $v > v_c$ the oscillations of the transmission functions are different, so the attenuation of the high frequencies is not the same. Figure 4 shows the results of this analysis for the May 10, 1994 ozone measurements. The left panel of the figure shows the dial ozone profile compared with two ozonesonde smoothed profiles: the first with the range resolution Δz of the dial signals, while the other is filtered with a low-pass 2nd order polynomial fitting procedure. The number $N(z)$ of fitting range cells is determined by the cut-off frequency $v_c(z)$ of the dial smoothing procedure. Note that the smoothing procedure reduces the maximum altitude of the ozonesonde profile. The right panel of the figure shows the differences between the dial and the ozonesonde profiles in the two cases. The smoothing procedure of the ozonesonde profile reduces the difference between the two ozone profiles but this difference remains high especially in the lower stratosphere (up to 30%). This difference can be explained only in part by the different air mass sampled by the two instruments and a different behaviour of the smoothing procedures and it is related to the two different kinds of ozone profile measurements. Similar differences are reported in other papers where ozone concentration values, obtained with different instruments, are compared (Beekman *et al.*, 1994; Hilsenrath *et al.*, 1986).

3. Aerosol backscattering ratio algorithm

Lidar stratospheric aerosol measurements are usually obtained by elastic backscattering. It is often convenient to analyse lidar aerosol data in term of the backscattering ratio. The aerosol backscattering ratio is defined as the ratio of total backscatter and molecular backscatter as follows

$$R_\lambda(z) = \frac{\beta_{a,\lambda}(z) + \beta_{R,\lambda}(z)}{\beta_{R,\lambda}(z)}. \qquad (3.1)$$

To obtain the backscattering ratio $R_\lambda(z)$, the lidar signal in eq. (2.1) is compared with the molecular signal calculated from an atmospheric density profile available from radiosonde soundings or atmospheric models. Making the ratio of the real signal with the molecular signal the backscattering ratio $R_\lambda(z)$ can be rewritten as

$$R_\lambda(z) = K \frac{S_\lambda(z)}{S_{M,\lambda}(z)} \exp[2\tau_{a,\lambda}(z)] \qquad (3.2)$$

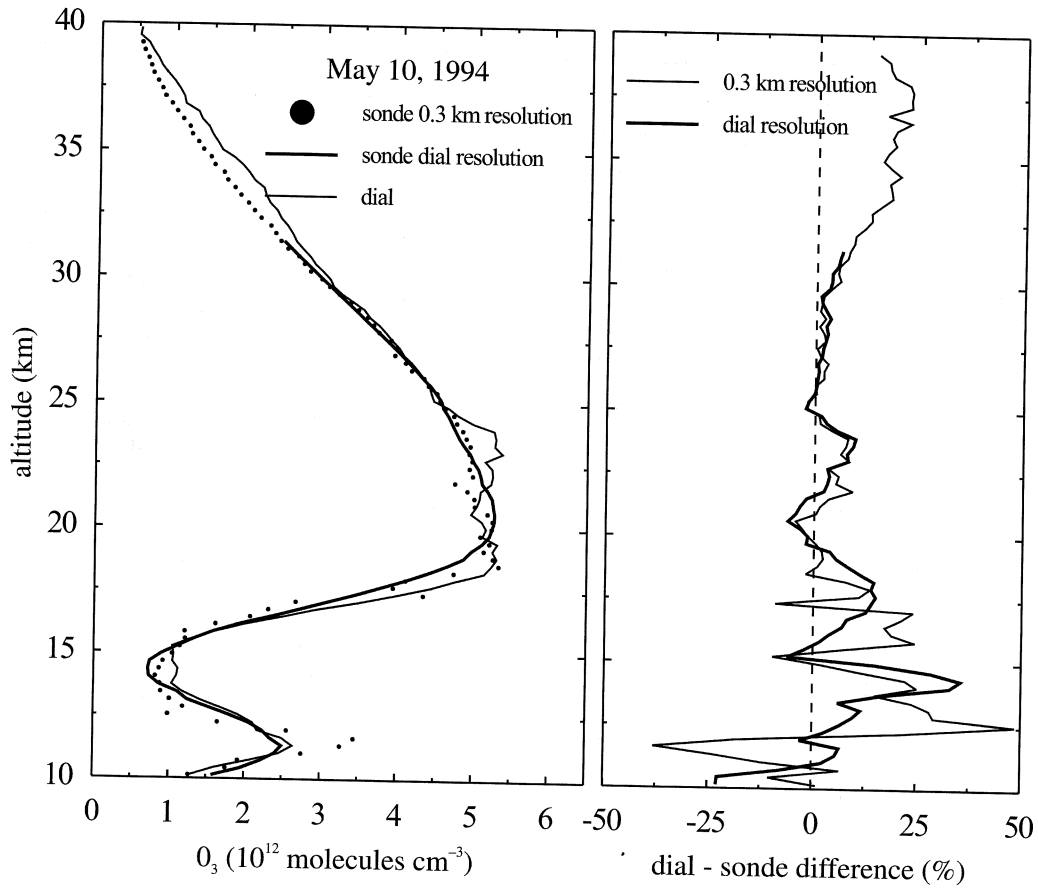

Fig. 4. *Left:* May 10, 1994 dial ozone profile compared with two smoothed ozonesonde profiles. Black dots reproduce ozonesonde profile 0.3 km smoothed while the thick line reproduces the ozonesonde profile with the same range resolution as the dial ozone profile (thin line). *Right:* differences between ozonosonde and dial profiles in the two cases.

where $\tau_{a,\lambda}(z)$ is the aerosol optical depth and $S_{M,\lambda}(z)$ is the molecular reference signal from range z. If the lidar signal is collected at a wavelength with a high ozone absorption (*i.e.* 308 nm) the reference signal $S_{M,\lambda}(z)$ must be calculated also taking into account the ozone absorption. This introduces a high error on the retrieved backscattering ratio values as will be seen later. The constant K can be obtained normalising $R_\lambda(z)$ to the value 1 above the aerosol layer (typically 30-35 km altitude range) where $\beta_{a,\lambda}(z) = 0$. The aerosol optical depth $\tau_{a,\lambda}(z)$ can be written as follows

$$\tau_{a,\lambda}(z) = \frac{3}{8\pi}\sigma_{R,\lambda}C_\lambda \int_0^z \rho(z')[R_\lambda(z') - 1]dz' \quad (3.3)$$

where $\sigma_{R,\lambda}$ is the Rayleigh scattering cross section at wavelength λ, $\rho(z)$ is the atmospheric number density, and C_λ is the extinction to backscattering ratio which is assumed constant with z. The eq. (3.3) contains $R_\lambda(z)$, so the resulting expression obtained combining eq. (3.2) and eq. (3.3) can be solved with an iterative approach.

In the first step $R_\lambda(z)$ is calculated assuming $\tau_{a,\lambda}(z) = 0$ and used in the second step to calculate $\tau_{a,\lambda}(z)$. In a generic step $R_\lambda(z)$ is obtained using $\tau_{a,\lambda}(z)$ calculated in the previous step. The process is repeated until the values of $R_\lambda(z)$ converge. The aerosol backscattering ratio standard deviation is given by

$$\sigma_R^2(z) = R_\lambda^2(z)\left[\frac{\sigma_K^2}{K^2} + \frac{\sigma_{S_\lambda}^2(z)}{S_\lambda(z)^2} + \frac{\sigma_\rho^2(z)}{\rho(z)^2} + \right. \tag{3.4}$$

$$\left. + 4\sigma_{\tau_{R,\lambda}}^2(z) + 4\sigma_{\tau_{a,\lambda}}^2(z) + 4\sigma_{\tau_{oz,\lambda}}^2(z)\right]$$

where the optical depth variances are calculated as in Russel *et al.* (1979). The last term in eq. (3.4) is relevant for wavelengths where ozone absorption is high (308 nm for SLAQ) as can be seen in fig. 5. The left panel of this figure shows the aerosol backscattering ratio profiles obtained at SLAQ on November 11, 1991 five months after the Pinatubo eruption. The features of the Pinatubo aerosol layer are well represented in all three available lidar signals. The right panel of fig. 5 shows the errors (1 σ standard deviation) of the aerosol backscattering ratio profiles. Note the high 308 nm backscattering ratio errors due to the correction for ozone extinction.

To calculate the aerosol optical depth $\tau_{a,\lambda}(z)$, the C_λ's value must be assumed. In any case

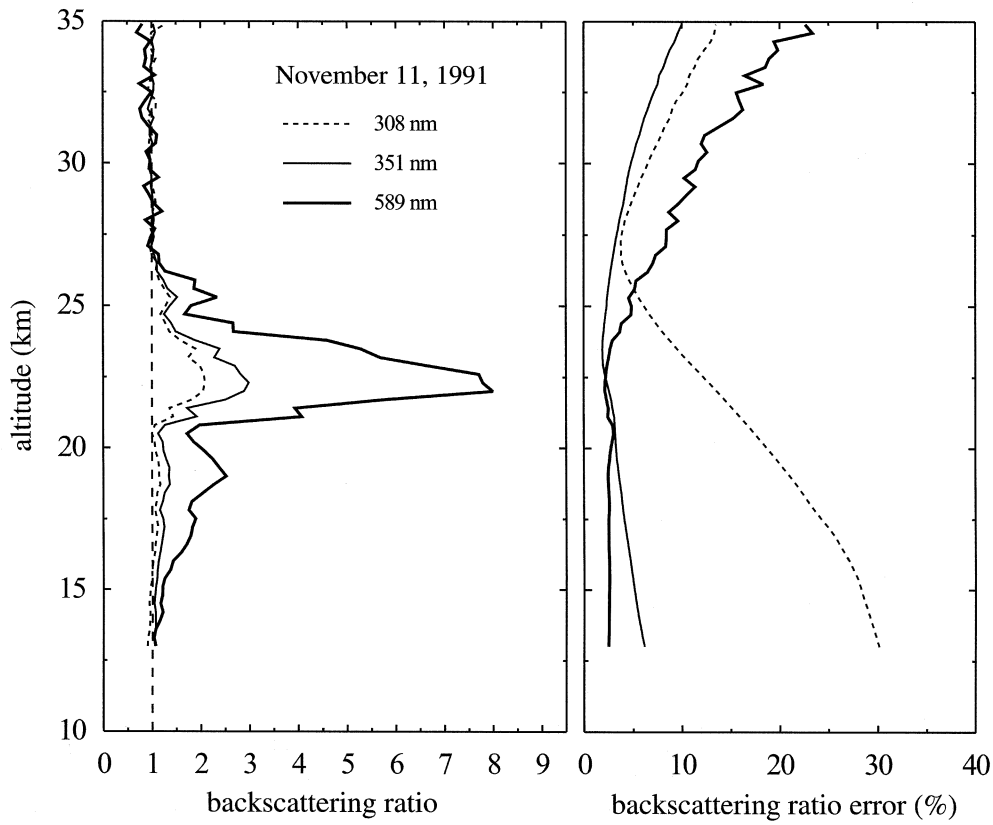

Fig. 5. Backscattering ratio profiles at 308 nm, 351 nm and 589 nm wavelengths with the respective errors (1σ standard deviation). The data refer to the measurements taken on November 11, 1991.

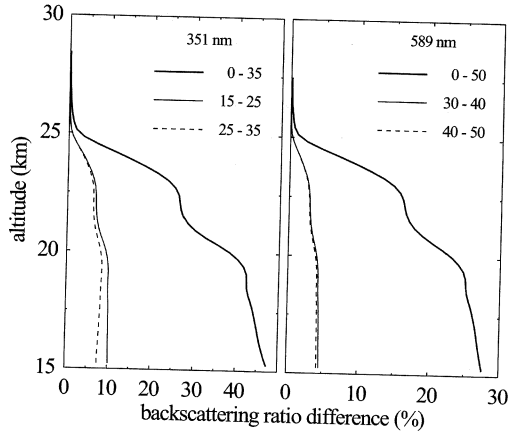

Fig. 6. Sensitivity test concerning the assumption of the C_λ's value in the aerosol backscattering ratio algorithm. See text for details.

after an explosive volcanic eruption C_λ ranges between [30 ÷ 50sr] for visible wavelengths and between [15 ÷ 35sr] for UV wavelengths (Jäger and Hofmann, 1991; D'Altorio *et al.*, 1993b). Figure 6 shows sensitivity tests concerning the assumption of C_λ's values for λ = 351 nm and λ = 589 nm respectively. The data refer to the measurement session reported in fig. 5. In both the panels the thick line reproduces the percentage difference between the backscattering ratio obtained without the aerosol extinction term (C_λ = 0sr) and the backscattering ratio calculated using the higher of the C_λ's values previously reported (C_{351} = 35sr, C_{589} = 50sr). The other curves reproduce the percentage difference between the backscattering ratios calculated using the boundary values of the interval previously reported (15sr and 35sr for 351 nm, 30sr and 50sr for 589 nm) and the backscattering ratios calculated using the middle values (C_{351} = 25sr, C_{589} = 40sr). It can be noted that neglecting the aerosol transmission loss, $R_\lambda(z)$ can be overestimated up to 45% in the UV wavelength and up to 25% in the visible wavelength, while assuming a C_λ's value in the previous intervals can introduce an uncertainty on the backscattering ratio values below 10% in the UV wavelength and below 5% in the visible wavelength.

4. Atmospheric temperature algorithm

Other information that can be obtained by elastic lidar returns is the atmospheric temperature profile in the stratosphere. This technique needs to have a lidar signal at a wavelength in which the ozone absorption can be neglected (*i.e.* 351 nm and 532 nm for SLAQ). In this approximation the lidar equation can be written as follows

$$S_\lambda(z) = \frac{k_\lambda}{z}\sigma_{R,\lambda}\rho(z)\exp\left[-2\sigma_{R,\lambda}\int_0^z \rho(z')dz'\right] \tag{4.1}$$

where $\sigma_{R,\lambda}$ is the Rayleigh scattering cross section at wavelength λ and $\rho(z)$ is the atmospheric number density at range z. In eq. (4.1) $3/(8\pi)$ is included in k_λ. Two steps are used in this technique. First a density profile is retrieved from the lidar signal. To do this the lidar signal is normalised at an altitude z^* where the density value is obtained by a model or a coincident radiosonde profile. Taking the ratio of eq. (4.1) writing for the generic altitude range z and for the reference altitude range z^* (with $z > z^*$) the density profile can be written as follows

$$\rho(z) = \rho(z^*)\left(\frac{z}{z^*}\right)^2 \frac{S(z)}{S(z^*)}\exp\left[2\sigma_{R,\lambda}\int_{z^*}^z \rho(z')dz'\right]. \tag{4.2}$$

This expression, like eq. (4.1), assumes no contribution from aerosol either in backscattering or extinction and includes the term of molecular atmospheric transmission. In this assumption the normalising altitude z^* is taken above the stratospheric aerosol layer, typically near 30 km. Then a relative density profile can be obtained by eq. (4.2) assuming the density value at the altitude z^*. Since the transmission term also contains the atmospheric density value, the eq. (4.2) can be solved with an iterative approach. A first guess is made for the atmospheric density value at altitude z^*. For the other altitudes over z^*, in the first step the transmission term is calculated using the density value at

the previous altitude. So a new value of density is calculated. The process is repeated from three to six times until the value of density at the current altitude converges. Since the lidar signal must be normalised at z^*, the absolute density profile depends on the density value at this reference point. However the relative density profile $\rho(z)/\rho(z^*)$ depends only on the lidar signals and does not depend on the density reference value. As it will be seen later, the retrieved temperature profile depends on the relative density profile. Therefore the retrieved temperature profile does not require an accurate value for the reference density. The second step is to compute the temperature profile using the ideal gas law and assuming the atmosphere is in hydrostatic equilibrium. First the hydrostatic equation is integrated from z to z_n ($z < z_n$) where z_n is the altitude corresponding to the n^{th} layer of the atmosphere. Second the resulting expression, in terms of atmospheric pressure, is substituted into the ideal gas law. The final expression of the ideal gas law, solved for temperature, can be written as follows

$$T(z) = T(z_n)\frac{\rho(z_n)}{\rho(z)} + \frac{M}{k_b \rho(z)} \int_z^{z_n} \rho(z')g(z')dz' \tag{4.3}$$

where M is the mean molecular mass of air, k_b is the Boltzmann constant and $g(z)$ is the acceleration due to the gravity. The integral in eq. (4.3) can be approximated using the trapezoidal rule, so the temperature standard deviation is given by

$$\sigma_T^2(z) = \frac{1}{\rho^2(z)} \cdot \left[T^2(z)\sigma_\rho^2(z) + \rho^2(z_n)\sigma_T^2(z_n) + \right. \tag{4.4}$$
$$\left. + T^2(z_n)\sigma_\rho^2(z_n) + \left(\frac{M}{k_b}\right)^2 \sigma_I^2(z) \right]$$

where $\sigma_I(z)$ represent the standard deviation of the integral present in the eq. (4.3). Thus by specifying the temperature $T(z_n)$ at the reference altitude z_n is possible to derive the temperature profile between z^* and z_n. To reduce the statistical error a smoothing procedure is performed on the final temperature profile as in the dial algorithm. In this case a running linear fitting is applied on the temperature profile $T(z)$ over a number $N(z)$ of range cells above and below z. Then the final temperature profile is given by

$$T_f(z) = a_0 + a_1 z \tag{4.5}$$

where a_j (j = 0,1) are the fitting coefficients. Therefore the final temperature standard deviation is given by

$$\sigma_{T_f}^2(z) = \sigma_{a_0}^2(z) + z^2\sigma_{a_1}^2(z) + 2z\sigma_{a_0,a_1}^2(z) \tag{4.6}$$

where $\sigma_{a_j}^2(z)$ are the variances of the fitting coefficients and $\sigma_{a_0,a_1}^2(z)$ is the covariance of a_0 and a_1. Applying on temperature profile a smoothing procedure is equal to apply a low-pass nu-

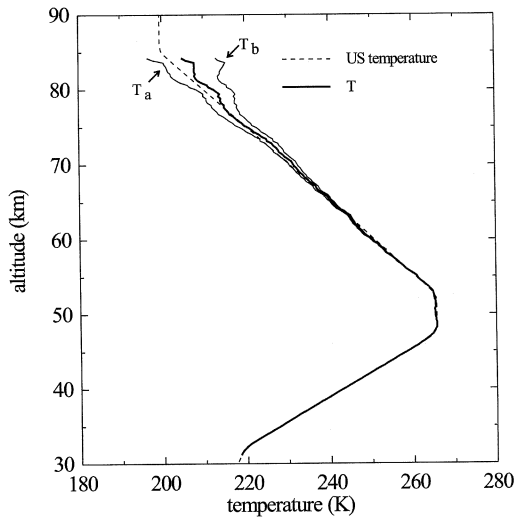

Fig. 7. Temperature profiles retrieved from model lidar signal at 351 nm changing the reference temperature value compared with the initial temperature profile (dashed line). T curve: right reference temperature value. T_a and T_b curves are obtained decreasing and increasing the reference temperature value by 10%.

merical filter on it to eliminate noise. So the range resolution of the temperature profile is given by eq. (2.13) where $v_c(z)$ are now the cut-off frequencies of the linear low-pass filter.

In this technique, to obtain the atmospheric temperature profile a reference temperature value $T(z_n)$ must be assumed. This assumption influences the retrieved temperature profile, but this influence decreases rapidly with altitude, and is negligible at altitudes about 20 km below z_n as can be seen in fig. 7. To illustrate this point more clearly, a temperature profile was retrieved from a model lidar signal at 351 nm. The temperature reference altitude was fixed at 90 km. Figure 7 shows the US Standard Atmosphere temperature profile and the temperature profile (curve T) retrieved using the right temperature reference value. The other temperature curves T_a and T_b, are obtained increasing and decreasing the reference temperature value by 10%. It can be seen that the three temperature profiles converge to the same value about 20 km below the reference temperature altitude. Note that the smoothing procedure reduces the maximum altitude of the retrieved temperature profiles with respect to the reference altitude. Figure 8 shows

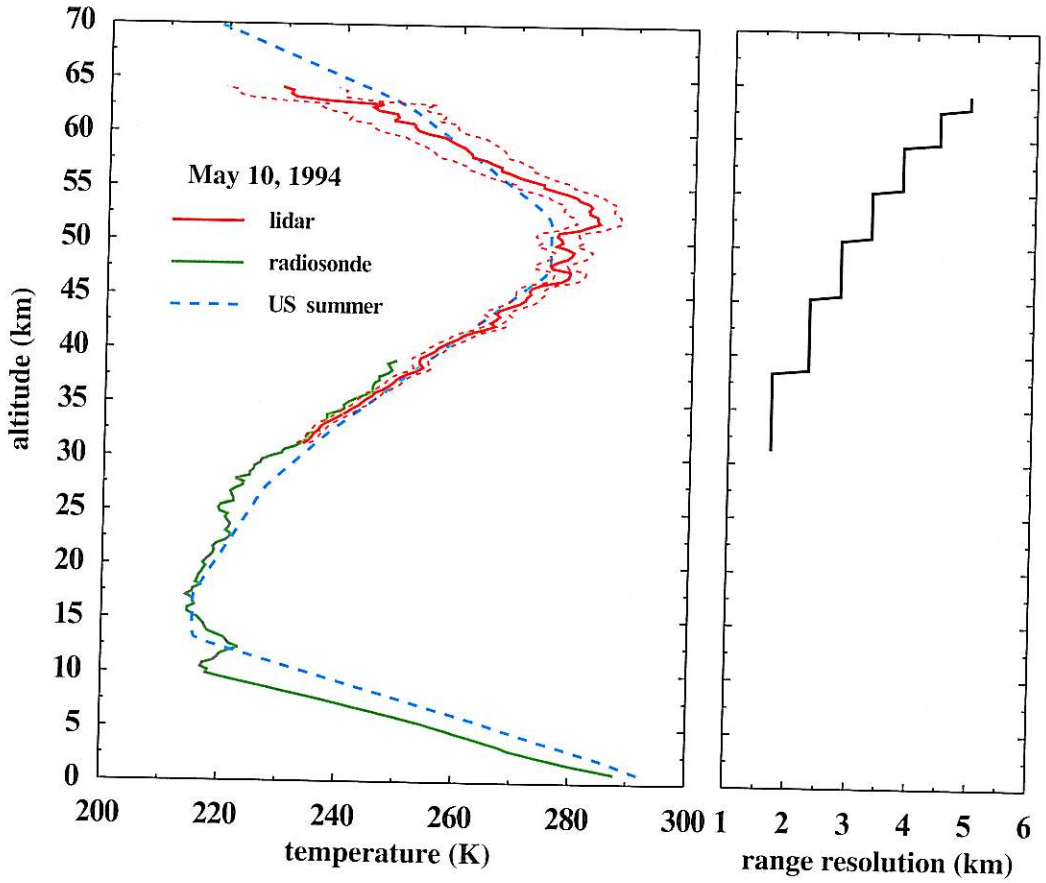

Fig. 8. *Left:* temperature profile (red line) retrieved from the May 10, 1994 351 nm lidar signal compared with the radiosonde temperature profile (green line) and the US Standard Atmosphere summer temperature profile (blue dashed line). Red dashed lines on either side of the lidar temperature profile denote the 1σ uncertainty in the derived temperature values. *Right:* range resolution of the lidar temperature profile.

the temperature profile retrieved from the 351 nm lidar signal obtained on May 10, 1994. The left panel of the figure shows the temperature lidar profile with the 1σ uncertainty, compared with the radiosonde temperature profile obtained in the same time period of the lidar measurement. The two profiles show a good agreement in the overlap altitude range (30-40 km). Figure 8 also shows the US Standard Atmosphere summer temperature profile. It can be noted that the lidar temperature values are consistent with the model temperature values. Both the sonde and the lidar profiles show similar differences with the model profile due to the daily fluctuations of the temperature values. The right panel of the figure also shows the temperature profile range resolution due to the smoothing procedure. The lidar temperature profile shown in fig. 8 is only an example to complete the set of measurements (ozone, aerosol backscattering ratio and temperature) obtained by a dial ozone system in a single session of measurement. In the case of the May 10, 1994 measurement the dial system was not optimised for high altitude temperature measurements. The future setup of the SLAQ's lidar systems will produce temperature profiles from 351 nm and 532 nm lidar signals up to higher altitudes and with a minor error respect to the temperature profile shown in fig. 8.

5. Conclusions

The check of the dial ozone algorithm with model lidar signals shows that the 3rd order polynomial fitting distorts the ozone profile less than the 1st and the 2nd order polynomial fitting procedures except for the higher altitude where the signal-to-noise ratios of the lidar signals are lower. Applying the algorithm on the SLAQ dial signals, the 3rd order polynomial fitting procedure shows similar results, but the error on the retrieved ozone values is up to four times higher than the lower order polynomial fitting procedures. So, the 2nd order polynomial smoothing procedure seems to give good results taking into account both distortions on the ozone profile and the error of the ozone values. The aerosol backscattering ratio algorithm has been tuned to take care of the aerosol transmission loss assuming the value of the aerosol extinction to backscattering ratio. This assumption reduces the uncertainty on the backscattering ratio values below 10% in the UV wavelengths and below 5% in the visible wavelengths. The temperature algorithm is checked with a model lidar signal at 351 nm to disclose the influence of the temperature reference value on the temperature profile. It is shown that the temperature profile does not depend from the reference value 20 km below the reference temperature altitude.

Acknowledgements

The Lidar Station of L'Aquila is a joint effort between the University of L'Aquila and the Istituto Nazionale di Geofisica (ING). The author thanks Prof. E. Boschi, President of ING, and Dr. B. Zolesi for the constant support and encouragement, Dr. V. Rizi, Prof. A. D'Altorio, Prof. G. Visconti and Dr. A.R. Pantaleo for suggestions and experimental work.

REFERENCES

BEEKMANN, M., G. ANCELLET, G. MEGIE, H.G.J. SMIT and D. KLEY (1994): Intercomparison campaign of vertical ozone profiles including electrochemical sondes of ECC and Brewer-Mast type and a ground based UV-differential absorption lidar, *J. Atmos. Chem.*, **19**, 259-288.

BUCHOLTZ, A. (1995): Rayleigh-scattering calculations for terrestrial atmosphere, *Appl. Opt.*, **34**, 2765-2773.

D'ALTORIO, A., F. MASCI, G. VISCONTI, V. RIZI and E. BOSCHI (1992): Simultaneous stratospheric aerosol and ozone lidar measurements after the Pinatubo volcanic eruption, *Geophys. Res. Lett.*, **19**, 393-396.

D'ALTORIO, A., F. MASCI, G. VISCONTI, V. RIZI and E. BOSCHI (1993a): Continuous LIDAR measurements of stratospheric aerosol and ozone after the Pinatubo eruption. Part I: DIAL ozone retrieval in presence of stratospheric aerosol layers, *Geophys. Res. Lett.*, **20**, 2865-2868.

D'ALTORIO, A., F. MASCI, V. RIZI, G. VISCONTI and M. VERDECCHIA (1993b): Continuous LIDAR measurements of stratospheric aerosol and ozone after the Pinatubo eruption. Part II: time evolution of ozone profiles and of aerosols properties, *Geophys. Res. Lett.*, **20,** 2869-2872.

DI CARLO, P., V. RIZI and G. VISCONTI (1998): Lidar observation of mesospheric sodium over Italy, *Nuovo Cimento C*, **21**, 541-549.

GODIN, S. (1987): Etude expérimentale par télédétection laser et modélisation de la distribution verticale

d'ozone dans la haute stratosphère, *Thèse de Doctorat de l'Université Pierre et Marie Curie, Paris.*

HILSENRATH, E., W. ATTMANNSPACHER, A. BASS, W. EVANS, R. HAGEMEYER, R.A. BARNES, W. KOMHYR, K. MAUERSBERGER, J. MENTALL, M. PROFFITT, D. ROBBINS, S. TAYLOR, A. TORRES and E. WEINSTOCK (1986): Results from the Balloon Ozone Intercomparison Campaign (BOIC), *J. Geophys. Res.*, **91**, 13137-13152.

JÄGER, H. and D.J. HOFMANN (1991): Mid-latitude lidar backscatter to mass, area and extinction conversion model based on *in situ* aerosol measurements from 1980 to 1987, *Appl. Opt.*, **30**, 127-138.

MALICET, J., D. DAUMONT, J. CHARBONNIER, C. PARISSE, A. CHAKIR and J. BRION (1995): Ozone UV spectroscopy. II. Absorption cross-sections and temperature dependence, *J. Atmos. Chem.*, **21**, 263-273.

MASCI, F., A. D'ALTORIO, V. RIZI and G. VISCONTI (1991): Preliminary results from the ozone lidar at the University of L'Aquila, *Nuovo Cimento C*, **14**, 651-654.

REDAELLI, G., L. LAIT, M. SCHOEBERL, P.A. NEWMAN, G. VISCONTI, A. D'ALTORIO, F. MASCI, V. RIZI, J. WATERS and J. MILLER (1994): UARS MLS O_3 soundings compared with lidar measurements using the conservative coordinate reconstruction technique, *Geophys. Res. Lett.*, **21**, 1535-1538.

RIZI, V., G. VISCONTI, A. D'ALTORIO and F. MASCI (1996): Comparing University of L'Aquila aerosol lidar measurements with LITE data, in *ELITE '94 Final Results Workshop Proceedings, IROE-CNR, Florence, Italy*, 91-93.

RUSSEL, P.B., T.J. SWISSLER and M. P. MCCORMICK (1979): Methodology for error analysis and simulation of lidar aerosol measurements, *Appl. Opt.*, **18**, 3783-3797.

STEINBRECHT, W. and A.I. CARSWELL (1995): Evaluation of the effects of Mount Pinatubo aerosol on differential absorption lidar measurements of stratospheric ozone, *J. Geophys. Res.*, **100**, 1215-1233.

YUE, G.K., M.P. MCCORMICK, P.H. WANG, V. RIZI, F. MASCI, A. D'ALTORIO and G. VISCONTI (1995): Comparing simultaneous stratospheric aerosol and ozone lidar measurements with SAGE II data after the Mount Pinatubo eruption, *Geophys. Res. Lett.*, **22**, 1881-1884.

(received September 21, 1998;
accepted January 19, 1999)